Available online at www.sciencedirect.com
ScienceDirect
Polymer 48 (2007) 6622–6631
polymer
www.elsevier.com/locate/polymer

Emulsion polymerized polyaniline synthesized with dodecylbenzene-sulfonic acid and its electrorheological characteristics: Temperature effect

Seong Gi Kim [a], Jae Yun Lim [a], Jun Hee Sung [a], Hyoung Jin Choi [a,*], Yongsok Seo [b,*]

[a] Department of Polymer Science and Engineering, Inha University, Incheon 402-751, South Korea
[b] Intellectual Textile System Research Center and School of Materials Science and Engineering, Seoul National University, Seoul 151-744, South Korea

Received 31 May 2007; received in revised form 1 September 2007; accepted 7 September 2007
Available online 14 September 2007

Abstract

Dodecylbenzene-sulfonic acid (DBSA)-doped polyaniline (PANI) was prepared by emulsion polymerization, where DBSA was used as both an emulsifier and a dopant. The chemical structure and morphology of the DBSA were examined via FT-IR and SEM, respectively. Electrorheological (ER) properties of DBSA-doped PANI particles dispersed in silicone oil were studied under different operating temperatures and an applied electric field. Shear stress data as a function of shear rate fitted quite well with the Cho–Choi–Jhon (CCJ) shear stress model. Both deduced static and dynamic yield stresses were found to be collapsed into a universal scaling function. Furthermore, the Cole–Cole plot and the dielectric spectra gave relaxation times of the ER systems for different operating temperatures of dielectric measurements, confirming the correlation of dielectric properties with ER performance.

Keywords: Polyaniline; Electrorheological fluid; Yield stress

1. Introduction

Electrorheological (ER) fluids are colloidal suspensions of polarizable solid particles dispersed in a non-conducting liquid, exhibiting drastic and reversible change in rheological properties when an external electric field is applied via ordering of the microstructure into particulate columns [1–4]. Furthermore, their rheological characteristics and engineering performance can be accurately controlled by an external applied electric field. Due to these controllable and outstanding characteristics, they are regarded as intelligent and smart materials. This rapid and reversible response opens up numerous potential engineering applications in various electrically controlled mechanical devices that transform electrical energy to mechanical energy such as dampers, brakes, shock absorbers, and actuators [5].

The ER phenomenon can be explained by either a polarization or a conduction model, both of which have been well established as the basic mechanisms of the ER fluid. The polarization model is proposed based on the observation that the applied external field induces electric polarization within each particle relative to the suspending medium. The resulting electrostatic interaction between the particles leads to the formation of aggregates aligned in the direction of the field [6,7]. This aggregation of particles results in an increase of viscosity. In general, the polarization may arise from various charge transport mechanisms, such as orientation of atomic/molecular dipoles or interfacial polarization, with the latter being generally considered as the main contributor to the ER behavior under dc or ac fields. This basic model of particle polarization leading to aggregation and increased flow resistance appears to have gained general acceptance [2]. On the other hand, with a decreased gap between the conducting particles in the fluid,

* Corresponding authors.
E-mail addresses: hjchoi@inha.ac.kr (H.J. Choi), ysseo@snu.ac.kr (Y. Seo).

0032-3861/$ - see front matter © 2007 Elsevier Ltd. All rights reserved.
doi:10.1016/j.polymer.2007.09.013

the electric response of the fluid becomes nonlinear, *i.e.*, electrical breakdown or particle discharge at high electric field strength occurs. In this case, the ER effect is caused by fluid-induced conductivity enhancement among particles that are nearly in contact. The conductivity mismatch between particles and liquid media, rather than the dielectric constant mismatch, is considered to be a dominant factor for dc and low frequency ac excitation [8]. The conduction model considers the particle interaction only and does not take into account the microstructural changes that occur after the application of an electric field. In addition, it can be also noted that a polar molecular dominated ER mechanism was recently proposed to explain reported giant ER fluids [9,10].

Concurrently, considerable emphasis has been placed on the development of optimal materials for ER fluids, particularly anhydrous materials, which have a broad operating temperature range. Among various polarizable particles for anhydrous ER materials, semiconducting polymers including polyaniline (PANI) [11–13], *N*-substituted copolyaniline [14], sulfonated poly(styrene-*co*-divinylbenzene) [15], copolystyrene particles with a polyaniline coating [16], poly(aniline-*co*-*o*-ethoxyaniline) [17], and poly(acene quinone) radicals [18] have been investigated. Recently, polymer–inorganic nanocomposites [19–22] and conducting polymers/mesoporous silica hybrids [23–25] have been adopted as dry-based ER materials. Note that various inorganic materials have also been reported to exhibit excellent ER performance [26].

In this paper, we investigated dodecylbenzene-sulfonic acid (DBSA)-doped PANI synthesized via emulsion polymerization as a potential candidate for anhydrous particles in high performance dry-base systems [27]. However, after synthesis, most of the DBSA dopant of PANI will be removed in order to be used for ER material in a semiconducting regime. PANI has been mainly synthesized via either chemical oxidative or electrochemical polymerization. While electrochemical oxidation of aniline in aqueous acidic media lets PANI synthesis on metal or conducting glass electrodes, its possible synthesis of the exact emeraldine oxidation state is known to be complicated. Chemical oxidative polymerization is regarded to be a feasible route for the production of PANI on a large scale. On the other hand, emulsion polymerization of PANI is known to be one of the most effective methods to produce its particulate form. For this process, the concept of dopant engineering is adopted in the present work and surfactants that can act as both an emulsifier and a dopant are selected [28]. PANI–DBSA complexes are reported to be obtained with high molecular weight and high solubility. Rheological properties of these ER fluids prepared from DBSA-doped PANI are measured using a rotational rheometer equipped with a high-voltage generator. Furthermore, the effect of temperature on the ER performance of the PANI system is also assessed. It was recently reported that in the case of a Ce-doped silica system, the ER activity was enhanced significantly by increasing the temperature. Such increment of ER properties with temperature was caused by increases in the interfacial polarization and the thermally activated charge carriers, which result from Ce-doping [29].

2. Experimental

2.1. Synthesis of emulsion polymerized polyaniline

PANI is typically chemically synthesized in an acidic aqueous medium, to which an oxidant is added [30,31]. However, in the present work, DBSA-doped PANI was synthesized using an emulsion polymerization technique [27]. This polymerization is carried out in non-polar or weakly polar solvents in the presence of a functionalized protonic acid that acts simultaneously as a surfactant (or emulsifier) and as a protonating agent (dopant) for the resulting electrically conducting PANI [28]. For the emulsion polymerization of DBSA-doped PANI, a solution composed of 19.52 g (0.2 mol) of aniline, 97.92 g (0.3 mol) of DBSA, and 1 l of xylene was prepared in a 2 l reactor. The polymerization was initiated by the addition of 9.36 g (0.04 mol) of ammonium peroxysulfate, $(NH_4)_2S_2O_8$, in 80 ml distilled water, which was added over a period of 30 min in order to avoid overheating of the reaction mixture. The polymerization temperature was kept at 25 °C for 24 h. The polymerization was terminated by pouring 3 l of acetone into the emulsion system, leading to precipitation of the PANI–DBSA complex. A dark green powder of the synthesized polymer particle was recovered, filtered, and washed three times with 600 ml acetone, three times with 600 ml distilled water, and three more times with 600 ml acetone, sequentially. After these filtering and washing procedures, the PANI particles were ground using a pearl mill and passed through a 38 μm sieve to control the particle size and distribution.

Meanwhile, since the synthesized PANI particles themselves have a high conductivity, electrical short due to the high current density would occur during the ER measurement if the particles were applied directly as an ER material. Therefore, it is necessary to decrease the electrical conductivity of the PANI particles synthesized by decreasing their protonation level. To lower the conductivity of PANI and make semiconducting PANI for the present ER study, the PANI particles were dedoped by increasing the pH of the aqueous medium to 10 using an aqueous NaOH solution [32]. The pH of the aqueous PANI suspension was kept constant for 1 day. The pH-controlled particles were again filtered and washed using distilled water, ethanol, and cyclohexane to remove both oligomer and excess monomer and to render the particle surface hydrophobic.

Finally, the PANI products were dried in a vacuum oven at 25 °C. The conductivity of the PANI, prepared in a compressed disk shape, was measured to be 1.78×10^{-10} S/cm by the 2-probe method.

2.2. Preparation of ER fluids

The ER fluids were prepared by dispersing the synthesized DBSA-doped PANI particles (15 wt%) in silicone oil. The PANI particles were subsequently dried in a vacuum oven and stored in molecular sieves prior to use. The density of the silicone oil with a kinematic viscosity of 30 cS was

0.95 g/ml at 25 °C. The prepared ER fluids were stored in a dessicator prior to use. Before each measurement, all ER fluids were dispersed again by a mechanical stirrer.

2.3. Characterizations

Rheological measurements of a suspension of DBSA-doped PANI particles in silicone oil with and without an applied electric field were performed. Experiments were carried out using a Physica rheometer (MC 120) with a Couette geometry, a high-voltage generator, and an oil bath for temperature control. The suspension was placed in the gap between the stationary outer measuring cup and the rotating measuring bob. An electric field was applied for 3 min in order to obtain an equilibrium chainlike or columnar structure before applying the shear. All measurements were performed at 25 ± 0.1 °C. In order to obtain reproducible data, the ER fluid was redispersed before each experiment and measurements were carried out at least two or three times. The available shear rate was varied from 10^{-4} to 10^{3} s^{-1}. Yield stresses for the prepared ER fluid were mainly obtained from a flow curve, which was obtained by a controlled shear rate experiment. The stress of the transition point at which shear viscosity abruptly decreased was regarded as the yield stress.

Two types of shear tests were used to characterize the steady shear behavior of the ER fluid. Primarily, for the controlled shear stress (CSS) mode, the shear stress was determined by presetting the shear stress and recording the shear rate. In this measurement method, the torque, and thus the shear stress, was preset, and the resulting speed, and thus the shear rate, was measured. Second, the speed of the rotating bob, and thus the shear rate, was preset. The flow resistance was then measured as a torque, which could be converted into the shear stress (controlled shear rate (CSR) mode). On the other hand, in dynamic experiments, a sinusoidal strain was applied to the ER fluid by driving the cylindrical bob. The viscoelastic parameter of the storage modulus (G') was then automatically measured. Using the Physica universal measuring system described above and US200 software, two different experiments were performed. First, strain amplitude was swept from 0.001 to 100 at a fixed driving frequency. Second, the driving frequency was swept from 0.1 to 100 Hz at fixed strain amplitude.

For the conductivity measurement, the top and bottom sides of a pellet of each sample of dried PANI were coated with aluminum and the pellet was then placed between two electrodes. Voltage was applied and the current was then measured. The conductivity (σ) was calculated using the surface area (A), thickness (d), and resistance (R) of each pellet according to the following relationship: $\sigma = (1/R)(d/A)$.

Dielectric relaxation of the prepared ER fluid was observed using an HP 4284A Precision LCR meter with an HP 16452A Liquid Test Fixture at room temperature. Frequency of the ac electric fields varied from 20 to 1 MHz. The relative dielectric constant indicates the energy value of a material in an electric field. The HP 16452A and HP impedance analyzer/LCR meter use the ''capacitive method'' for obtaining relative permittivity by measuring the capacitance of a material that is sandwiched between parallel electrodes.

3. Results and discussion

Successful emulsion polymerization of PANI was confirmed by a Fourier transform infrared spectral (FT-IR) analysis. Fig. 1 shows the FT-IR spectrum of the DBSA-doped PANI, determined using KBr pellets. The peak at 825 cm^{-1} originates from the out-of-plane H deformation of aromatic rings in PANI unit sequences, whereas the peaks at 1145 and 1310 cm^{-1} are due to aromatic amine stretching, and those at 1490 and 1590 cm^{-1} are the C–C stretching modes. The FT-IR spectrum shows that the DBSA-doped PANI synthesized for this study is similar to that of an emeraldine base.

Particle size and shape of the DBSA-doped PANI produced were observed via SEM. Fig. 2 indicates that PANI particles have an irregular and plate-like structure with a particle size distribution. The size range of the particles is approximately 1–15 μm. This type of structure originates from the rigid molecular structure of the PANI.

Fig. 3 presents flow curves measured from the controlled shear rate mode, *i.e.*, shear stress as a function of shear rate for the DBSA-doped PANI based ER fluid (particle concentration of 15 wt%) for different applied electric fields up to 3.5 kV/mm. The shear stresses simply increased with applied electric field strength. However, the shear stresses of the ER fluid as a function of the shear rate range initially decrease and then increase again, while a broad plateau region over the entire shear rate range is observed for 0.5 kV/mm. In the low shear rate ($\dot{\gamma}$) region, the electrostatic interactions among particles induced by external electric fields are regarded to be dominant compared to the hydrodynamic interactions induced by the external flow field. The aligned particular structures begin to break apart with shear deformation. The broken structures tend to then reform in chains by the applied electric field, depending on the magnitude of the applied shear rate

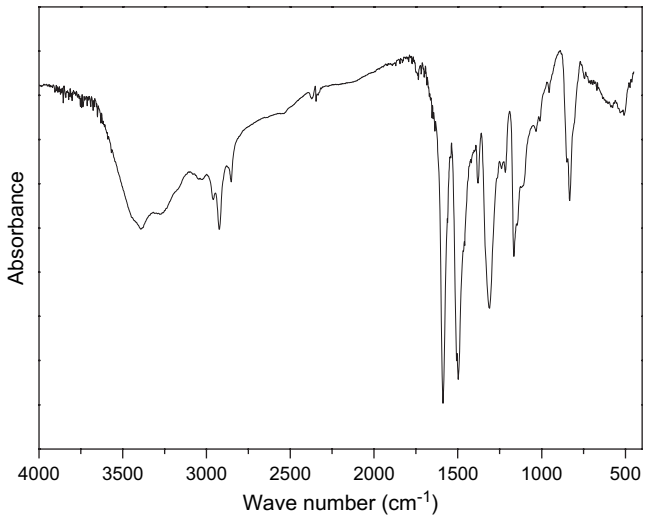

Fig. 1. FT-IR curve of the DBSA-doped PANI particles.

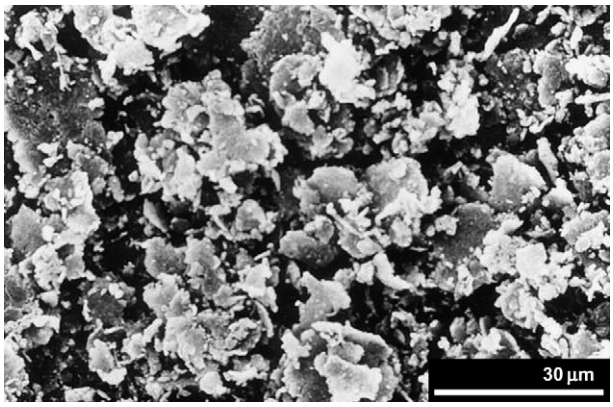

Fig. 2. SEM photograph of DBSA-doped PANI particles.

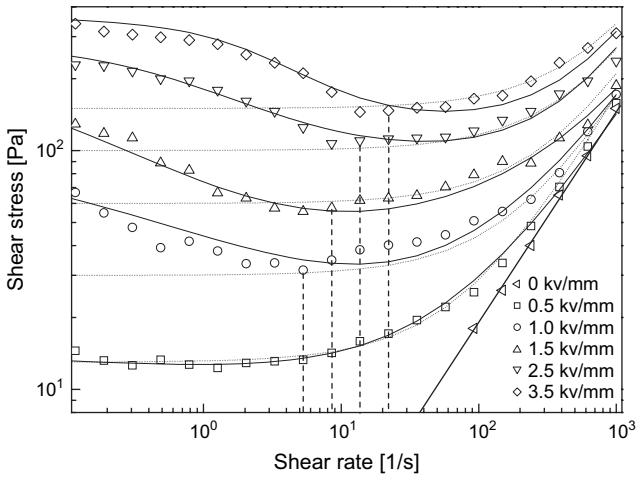

Fig. 3. Flow curve of shear stress *vs*. shear rate measured from the CSR mode for 15 wt% DBSA-doped PANI based ER fluids. Dotted line is for Bingham model, solid line for CCJ model, and vertical dashed line for the critical shear rate.

and particle–particle interaction in the fibrils. However, the decrease in shear stress (τ) is observed when the reformed structures of the dispersed ER particles at a higher $\dot{\gamma}$ are not as complete as those before applying shear flow [33,34]. The finding of a decrease of τ with increasing $\dot{\gamma}$ up to a critical shear rate ($\dot{\gamma}_{crit}$) has been reported for various ER materials [35–38].

$\dot{\gamma}_{crit}$ is a transition point of $\dot{\gamma}$ at which the fluid begins to exhibit pseudo-Newtonian behavior (τ increases with $\dot{\gamma}$). The ER fluid under five different applied electric fields exhibited similar behavior around $\dot{\gamma} = 10\,s^{-1}$, as shown in Fig. 3. In this $\dot{\gamma}$ range, the particle chains appear to be broken by the shear. Furthermore, there might be insufficient time for the particles to realign along the electric field direction [39]. In other words, as $\dot{\gamma}$ increases, the destruction rate of the fibrils becomes faster than the reformation rate. Finally, in the high shear rate range, the ER fluid shows liquid-like behavior, because the ER chains are fully broken. This phenomenon is related to the rate of polarization under the shear by an applied electric field and is discussed in conjunction with the dielectric spectral results given below.

On the other hand, the ER fluid shows solid-like behavior at high electric field strength with a residual shear stress, because the chain of ER particles resists the shear. As a result of this aggregated structure, ER fluids under an applied electric field are considered to exhibit Bingham fluid behavior possessing a yield stress (τ_y), which is defined as the stress extrapolated from the low shear rate region. The relationship between τ and $\dot{\gamma}$ for Bingham model is as follows [34]:

$$\tau = \eta_{pl}\dot{\gamma} + \tau_y \quad (\tau > \tau_y)$$
$$\dot{\gamma} = 0 \quad (\tau < \tau_y) \tag{1}$$

where η_{pl} is the plastic viscosity [40]. However, it is well known that the flow curves of many ER fluids deviate from Eq. (1). Complex shear stress behaviors such as a plateau region over a broad shear rate range, the existence of minimum shear stress at a relatively low shear rate region [41], and a coexistence region of a liquid–solid-like system [42], are often observed.

While there have been extensive studies involving quantitative analyses of both yield stress and shear stress behaviors [43,44], surprisingly, only a few reports on the constitutive equation can be found [44,45]. In order to examine this complex flow curve, a model constitutive rheological equation of state was suggested to more comprehensively analyze the ER fluids under an applied electric field in place of a quantitative interpretation [18].

The suggested Cho–Choi–Jhon (CCJ) model is given as follows:

$$\tau = \frac{\tau_y}{1+(t_1\dot{\gamma})^{\alpha}} + \eta_{pl}\left(1+\frac{1}{(t_2\dot{\gamma})^{\beta}}\right)\dot{\gamma} \tag{2}$$

This six-parameter model can cover the stress decrease phenomena at the low shear rate region and provide an accurate value of the real yield stress for various ER fluids. Here, α is related to the decrease in the stress, t_1 and t_2 are time constants, in which t_1 is considered to be the inverse of the shear rate at which the shear stress shows a minimum at a low shear rate region and t_2 is related to the inverse of the shear rate at which a pseudo-Newtonian behavior starts, and η_∞ is the viscosity at a high shear rate and is interpreted as the viscosity in the absence of an electric field. The exponent β falls in the range $0 < \beta \leq 1$, since $d\tau/d\dot{\gamma} \geq 0$ above the critical shear rate at which the shear stress becomes a minimum. The first term in Eq. (2) implies the shear stress behavior at a low shear rate region, especially in the case of a decrease of shear rate and the second term describes the shear stress behavior at a high shear rate region. The fitting of the model equation to the flow curve for DBSA-doped PANI based ER fluids is given in Fig. 3. The yield stresses and the optimal parameters for both Bingham and CCJ models are summarized in Table 1. The lines originated from the suggested constitutive equation model fit the flow curve data very accurately through the entire shear range, particularly the data investigated at a relatively

Table 1
The optical parameters in each model equation obtained from the flow curve of 15 wt% DBSA-doped PANI based ER fluids at various electric field strengths

Model	Parameter	0.5 kV/mm	1.0 kV/mm	1.5 kV/mm	2.5 kV/mm	3.5 kV/mm
Bingham	τ_y	13	30	60	100	150
	η_{pl}	0.158	0.14	0.15	0.17	0.19
CCJ	τ_y	20	120	250	170	190
	t_1	0.02	8	15	1.2	0.33
	α	0.1	0.34	0.5	0.8	1.2
	η_{pl}	0.09	0.1	0.09	0.18	0.2
	t_2	0.006	0.002	0.001	0.002	0.0017
	β	0.4	0.6	0.8	1.02	1.04

low shear rate. In contrast, Bingham model could not describe the data comprehensively but only provided a general outline.

Furthermore, a very important value for the ER fluid is the yield stress. The CSS method is known to be the best method to measure the yield stress, as this parameter is measured directly. From the flow curve $\tau = f(\dot{\gamma})$ of the CSR method, the yield stress is obtained from an intercept on the y-axis in the limit of $\dot{\gamma} \to 0$. Yield stress determined from the CSR method typically deviates from that obtained via the CSS method. This indicates that with a pseudo-plastic substance, very strong distortion in the flow curve appears, especially at very low shear rate.

On the other hand, the yield stress (τ_y) can be generally expressed as a non-analytic power law form of E as:

$$\tau_y = E_0^m \tag{3}$$

The obtained yield stresses of the PANI increase with applied electric field strength (E). The values of m in Eq. (3) for both static and dynamic yield stresses given in Fig. 4 range from 1.6 to 2.0. Fig. 4 presents the static and dynamic yield stresses *vs*. electric field strength for 15 wt% DBSA-doped PANI, obtained from the CSS mode and CSR mode measurements, respectively. These exponent m values are different from that obtained from the polarization model (*i.e*., 2.0) by falling in the region between $m = 1.5$ and $m = 2.0$, because the morphology of PANI is non-spherical and it has a broad particle size distribution, as can be seen in the SEM image (Fig. 2).

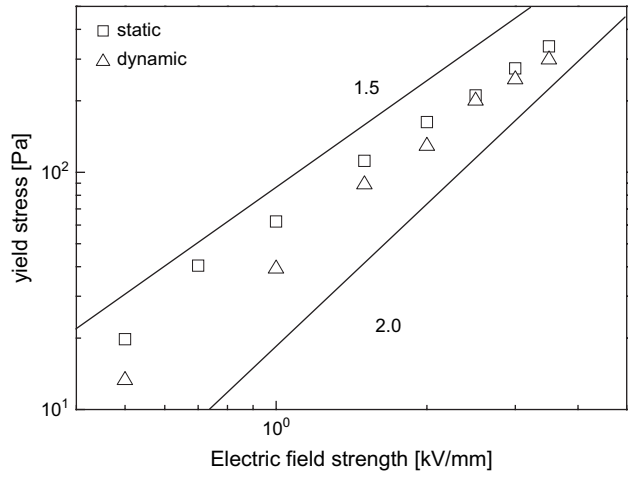

Fig. 4. Static and dynamic yield stresses *vs*. electric field strength in the CSS mode for 15 wt% DBSA-doped PANI based ER fluids bounded by two slopes of 1.5 and 2.0.

Note that the yield stress of ER fluid originates from the attractive forces between particles, by fully taking into account both the polarization and the conduction models. The polarization model, in general, relates the material parameters of ER fluids, such as the dielectric response of both liquid and solid particles and the electric field strength, to the rheological properties. Using an idealized ER system, in which uniform hard dielectric spheres are dispersed in a Newtonian fluid medium, the derived electrostatic force was found to be dependent on the dielectric constant mismatch between the particles and the continuous media [46,47]. Under these assumptions, the yield stress (τ_y) from the polarization model is found to be proportional to the square of the applied electric field strength. On the other hand, as the gap between the conducting particles in the fluid decreases, the electric response of the fluid becomes nonlinear, *i.e*., electrical breakdown or particle discharge at high electric field strength occurs. In this case, the ER effect is caused by the fluid-induced conductivity enhancement among nearly contacting particles. The conductivity mismatch between particles and liquid media, rather than the dielectric constant mismatch, is considered to be the dominant factor for the dc and low frequency ac excitation [48]. The conduction model considers the particle interaction only and does not take into account the microstructural changes that occur after application of an electric field, showing that the power law index "m" approaches 1.5 at high electric field strengths.

Recently, in order to represent the yield stress data for a broad range of electric field strengths, Choi et al. [49] introduced the critical electric field strength, E_c, into their simple hybrid yield stress formula to describe the deviation of the yield stress from the polarization model. Their proposed yield stress equation is written below.

A simple combined equation presents the yield stress data for a broad electric field strength range as follows:

$$\tau_y(E_o) = \alpha E_o^2 \left(\frac{\tanh \sqrt{E_o/E_c}}{\sqrt{E_o/E_c}} \right) \tag{4}$$

where α depends on the dielectric constant of the fluid, the particle volume fraction, and the dielectric constant mismatch

parameter. E_c is influenced by the conductivity mismatch between the particle and the liquid medium and is weakly dependent on the volume fraction. Generally, the correlation of τ_y with E_o is represented by the polarization model. E_c represents the critical electric field originating from the nonlinear conductivity model and is descriptive for crossover behavior and defines (or links) the two regimes in E_o *vs.* τ_y. The nonlinear conductivity effect is considered in a bulk conducting particle model, and the yield stress model fitting the power law index approaches 3/2 at high E. From this result, E_c indicates the different slope of correlation of E_o *vs.* τ_y [48]. Choi et al. [49] introduced the following universal yield stress equation to correlate yield stress with a broad range of electric field strength. Eq. (4) clearly possesses the following two asymptotic behaviors at low and high electric field strengths as compared to E_c with the following detailed derivations [50]:

$$\tau_y = \alpha E_o^2 \quad \propto E_o^2 \quad E_o \ll E_c \tag{5}$$

$$E_o \ll E_c; \quad \tanh\sqrt{E_o/E_c} = \left(\frac{E_o}{E_c}\right)^{1/2} - \frac{1}{3}\left(\frac{E_o}{E_c}\right)^{3/2} + \cdots \cong \left(\frac{E_o}{E_c}\right)^{1/2} \tag{5-1}$$

$$\therefore \tau_y(E_o) = \kappa E_o^2 \left(\frac{\sqrt{E_o/E_c}}{\sqrt{E_o/E_c}}\right) \quad \propto \quad E_o^2 \tag{5-2}$$

$$\tau_y = \alpha\sqrt{E_c}E_o^{3/2} \propto E_o^{3/2} \quad E_o \gg E_c \tag{6}$$

$$E_o \gg E_c; \quad \tanh\sqrt{E_o/E_c} = \left(\frac{E_o}{E_c}\right)^{1/2} - \frac{1}{3}\left(\frac{E_o}{E_c}\right)^{3/2} + \cdots \cong \left(\frac{E_o}{E_c}\right)^{1/2}$$

$$\therefore \tau_y(E_o) = \kappa E_o^2\sqrt{E_o/E_c}\left(\frac{e^{\sqrt{E_o/E_c}} - e^{-\sqrt{E_o/E_c}}}{e^{\sqrt{E_o/E_c}} + e^{-\sqrt{E_o/E_c}}}\right) \tag{6-1}$$

$$= \kappa E_o^2\sqrt{E_o/E_c} = \kappa\sqrt{E_c}E_o^{3/2} \quad \propto \quad E_o^{3/2} \tag{6-2}$$

Eq. (4) shows that τ_y is proportional to E_o^2 (Regime I) for low E_o and τ_y changes abruptly to $E_o^{3/2}$, transferring to Regime II for high E_o. E_c stems from the nonlinear conductivity model and represents the crossover behavior. E_c appears to be proportional to the particle conductivity and is influenced by the conductivity mismatch between the particle and the liquid medium and is weakly dependent on the volume fraction.

The response of the ER fluid becomes nonlinear through electrical breakdown at high electric field strengths. The polarization forces between particles increase with both increasing electric field strength and particle concentration. The conductivity among the stationary adjacent particles affects the ER response resulting from the conduction model [46].

Therefore, the slope in Fig. 4 can be decomposed into two parts, as replotted in Fig. 5. The change of the slope of the yield stress shows the critical electric field (E_c) at 0.6 kV/mm for the static mode and at 0.7 kV/mm for the dynamic mode. The yield stress depends on the E_o range, showing a value of 2 until reaching the critical electric field strength (E_c), and generally becomes smaller than 2 as $E_o > E_c$ [15]. The interfacial polarization is reported such that fibril structures are formed by the particle's rotation under an external electric field [47]. From the nonlinear conductivity model for ER fluids, good agreement of universal scaling is found between the predicted and the measured ER behaviors for various ER systems. The slope of the electric field E_o *vs.* τ_y (on log scale) is 3/2 at larger E_c, while the slope approaches 2 for smaller than E_c.

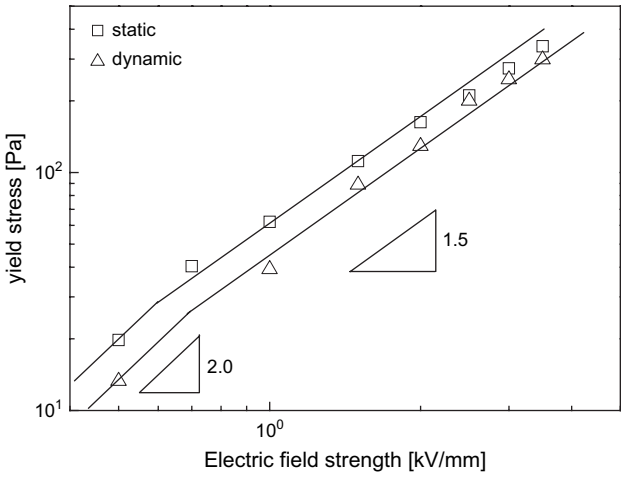

Fig. 5. Replotted static and dynamic yield stresses *vs.* electric field strength in the CSS mode for 15 wt% DBSA-doped PANI based ER fluids.

A single universal curve in Eq. (4) with E_c and $\tau_y(E_c)$ is normalized to collapse the data.

$$\tau_y(E_c) = \alpha E_c^2 \tanh(1) = 0.762\alpha E_c^2 :$$

$$\hat{\tau} = 1.313\hat{E}^{3/2}\tanh\sqrt{\hat{E}} \tag{7}$$

where $\hat{E} \equiv E_o/E_c$ and $\hat{\tau} \equiv \tau_y(E_o)/\tau_y(E_c)$. E_c shows different behavior at low and high electric field strengths by the normalized scaling function. Even though the proposed correlations of Eqs. (4) and (7) are not derived from first principles, they are important for representing data by experimentalists. The beauty of these correlations is the fact that most of the ER experimental data can be collapsed with a parameter E_c which is qualitatively related to particle properties and conductivity mismatch.

Fig. 6 shows the universal scaling curve of the DBSA-doped PANI based ER fluids with different yield stress modes. The universal curves collapse to a single line regardless of the yield stress modes.

Fig. 7 presents flow curves measured from the CSR mode for 15 wt% DBSA-doped PANI based ER fluids at an electric field strength of 1.0 kV/mm and various operating temperatures. Fig. 8 gives the static yield stress *vs.* operating temperature from the controlled shear stress mode.

In the practical application of ER fluids, sustained ER activity over a range of temperature is definitively needed.

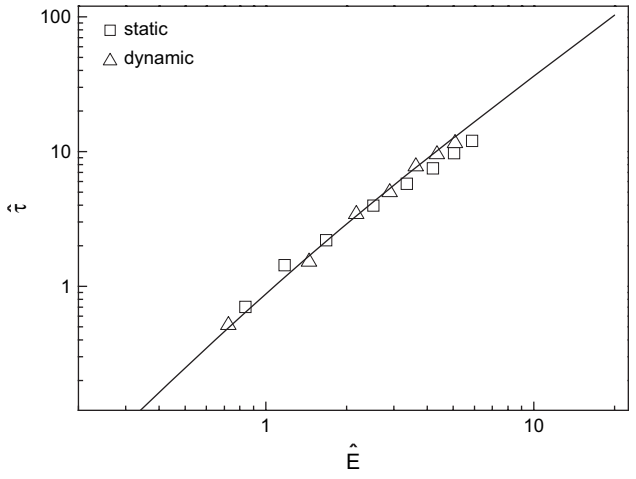

Fig. 6. Universal curve for $\hat{\tau}$ *vs.* $\hat{E}$ for yield and dynamic yield stress of 15 wt% DBSA-doped PANI based ER fluids.

In the case of a water-activated ER suspension, temperature elevation causes the evaporation of adsorbed water and consequently the ER effect decreases as the suspension temperature increases. However, although the zero-field viscosity of our dry-base DBSA-doped PANI based ER suspension clearly decreased with increasing temperature, given that the silicone oil viscosities were measured to be 30.6, 20.9, 14.8 and 11 mPa S for 20, 40, 60 and 80 °C, respectively, the dynamic yield stresses of the ER fluid increased somewhat with temperature. This is because the ER activity of the suspension arises mainly from the bulk property of DBSA-doped PANI particles. Namely, enhancement of conductivity due to temperature increment is caused by increasing the polarization force of the chain structure. However, for the present system of DBSA-doped PANI dispersed in silicone oil of 30 cS, an upper limit for the temperature is imposed by the current overload due to a conductivity enhancement with a rise in temperature. In this regard, the experimental data presented in Figs. 7 and 8 were obtained until the temperature reached a value at which current overload occurred.

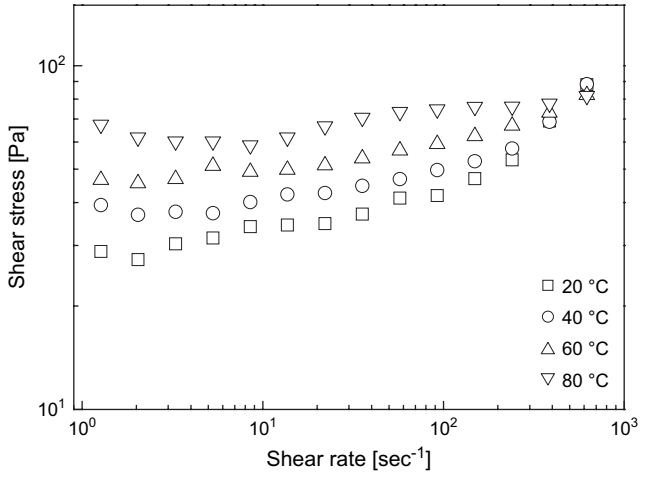

Fig. 7. Shear stress *vs.* shear rate measured from the CSS mode for 15 wt% DBSA-doped PANI based ER fluids at various operating temperatures and an electric field strength of 1 kV/mm.

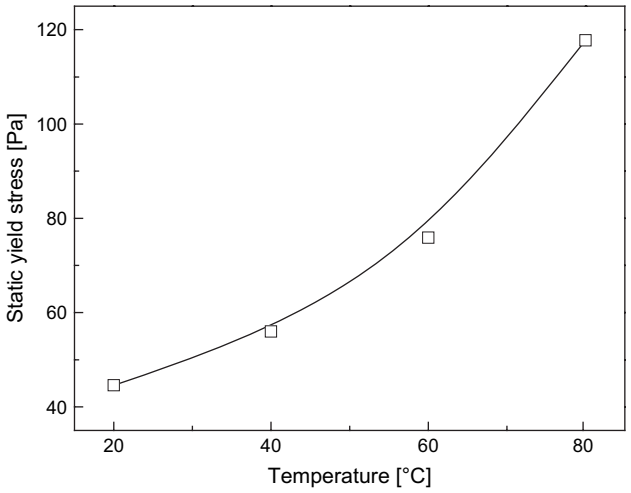

Fig. 8. Static yield stress *vs.* operating temperature measured from the CSS mode for 15 wt% DBSA-doped PANI based ER fluids at an electric field strength of 1 kV/mm.

It should also be noted that several factors are associated with the temperature effect on the ER performance. First, increased temperature tends to increase the current density and the increased dielectric constant or conductivity then enhances the particle's polarization, resulting in increased ER performance. On the other hand, increased temperature intensifies the thermal motion of the dispersed ER particles, which leads to lower stability and accordingly degrades the ER performance. Meanwhile, increased temperature also decreases the viscosity of the silicone oil. In general, high medium viscosity and higher ER fluid concentration cause a large frictional force, which makes it difficult for the dispersed particles to turn along the direction of the applied electric field and to form fibrillar chains. Therefore, decreased medium viscosity due to temperature increase makes chain formation relatively easy and thus leads to improved ER fluid strength. The ultimate ER effect comes from the balance attained among these factors, ultimately increasing the ER performance [51–55].

On the other hand, it has been reported that the stress response of an ER fluid subjected to a sinusoidal strain of small amplitude and an intermediate electric field shows a linear viscoelastic behavior. The amplitude and phase angle of the stress are dependent upon the applied electric field strength [56]. The response, however, becomes nonlinear with increasing strain amplitude due to breaking of the chain structure induced by the electric field. To sum up, the viscoelastic parameters of ER fluid with electric field strongly depend upon the strain amplitude.

Fig. 9 shows a plot of G' for the 15 wt% DBSA-doped PANI particle based ER fluid as a function of frequency at a very small strain ($\gamma = 0.00125$) in a linear viscoelastic region under various electric fields. It is shown that the storage modulus is almost constant as the deformation frequency is increased to 100 Hz. This resembles the typical behavior of cross-linked rubbers [57] with solid-like high elasticity. Since the relaxation time for deformation was sufficiently long, it is expected that the interfacial polarized attractive chain

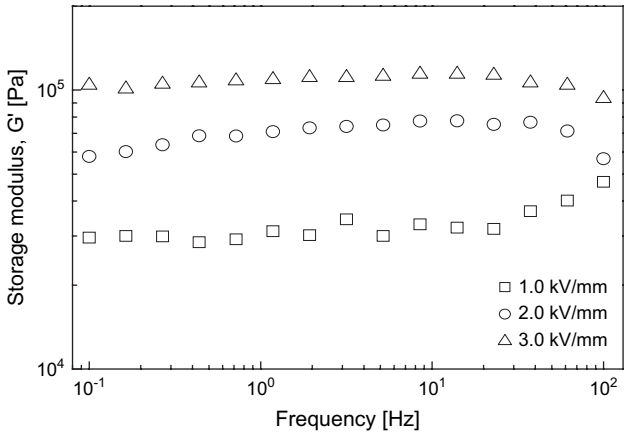

Fig. 9. G' as a function of frequency for 15 wt% DBSA-doped PANI based ER fluids at different electric field strengths and a strain of 0.00125.

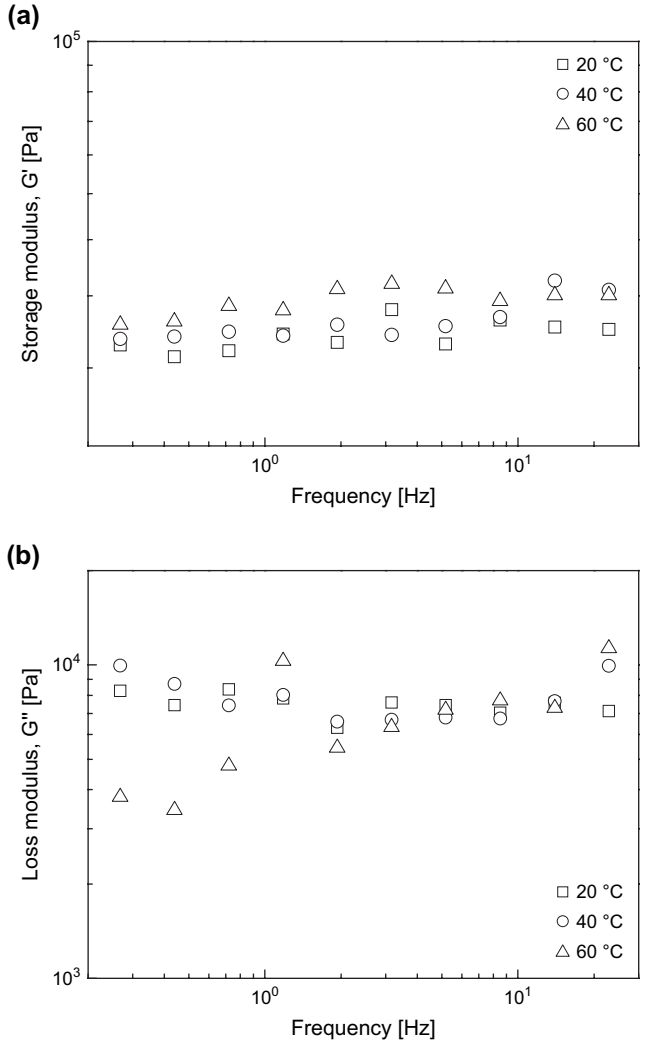

Fig. 10. G' (a) and G'' (b) as a function of frequency for 15 wt% DBSA-doped PANI based ER fluids with an electric field strength of 1 kV/mm at three different temperatures.

structures of the ER fluids were not destroyed by deformation under the given conditions. The increase in G' with the applied electric field indicates that the ER fluid becomes more elastic with the applied electric fields under the linear viscoelastic conditions with an exponent of 1.25 as a function of applied electric field [12].

In Fig. 10, G' for the 15 wt% DBSA-doped PANI particles based ER fluids is plotted as a function of frequency at a strain of 0.00125 for various operating temperatures at an applied electric field of 1 kV/mm in order to elucidate the effect of temperature on elasticity. It is observed that the elastic moduli (G') are slightly changed with different operating temperatures. However, not much difference was observed for the loss moduli (G'').

Several investigators [58,59] suggested that the interfacial polarization in a suspension of conducting particles in a non-conducting oil can be affected by the flow field and thus the ER phenomenon is the result of the interaction between the flow field and the polarization induced by an external electric field [60]. In order to study the mechanism of electrostatic interaction and the polarization properties of the present samples, we measured the dielectric spectra of the ER fluids in a frequency range from 20 to 10^6 Hz using an impedance analyzer.

Fig. 11(a) and (b) shows the dielectric properties (ε' and ε'') as a function of the electrical frequency for a 15 wt% DBSA-doped PANI based ER system at different operating temperatures. As expected, the magnitude of both ε' and ε'' increases and polarization of the ER fluid moves toward higher electrical frequency with increasing operating temperature. In particular, the dielectric constant of the ER suspension (ε') is considerably enhanced at low frequency due to the interfacial polarization.

Generally, the electrical conductivity of the ER fluid increases with increasing temperature. When the electrical conductivity of the particle is increased, ε', particularly at low frequency, is greatly enhanced, showing a maximum value. This is caused by facilitated interfacial polarization as a result of the increased mismatch in conductivity between the two phases. In the figures, dielectric relaxation is observed at 80 °C, as evidenced from the shape of ε' in Fig. 11(a) and the broad peak of ε'' in Fig. 11(b). The dielectric relaxation time, λ, of the polarization for the ER fluid can be obtained from the relation $\lambda = 1/(2\pi f_{\max}) \gg 4 \times 10^{-2}$ s, where $f_{\max} \gg 4$ Hz is the frequency when ε'' is maximal. ε' and ε'' for the ER fluid measured at 80 °C are significantly larger than those of the remaining ER fluid at low frequency. However, at a frequency much higher than the inverse relaxation time of the ER system, the dipole moment of the ER fluid can no longer follow the external electric field. Hence, it is observed that ε' and ε'' measured at different temperatures approach the same value at the high frequency limit. This relation between relaxation time and shear rate affects flow curve rather than yield stress of ER fluids reported here under an applied electric field, *e.g.*, decreases in the low $\dot{\gamma}$ region (Fig. 3). In general, suspended particles rotate around the applied shear field and the angular velocity (ω) is related to $\dot{\gamma}$ as $\omega \sim \dot{\gamma}/2$ [41]. Therefore, even under a dc electric field, particles or clusters that behave as if they were in an ac electric

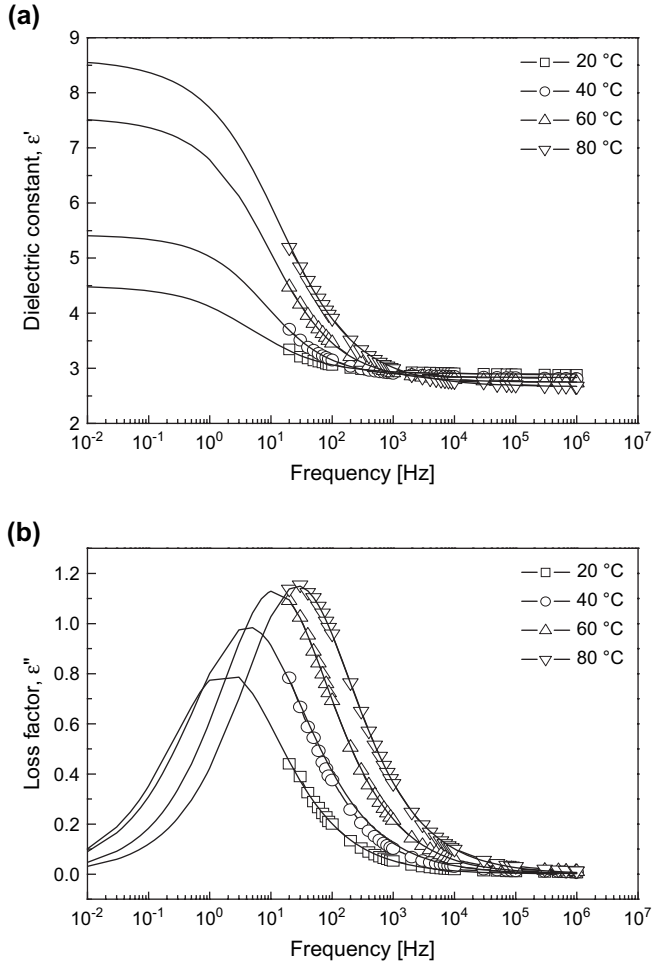

Fig. 11. ε' (a) and ε'' (b) as a function of electrical frequency for 15 wt% DBSA-doped PANI based ER fluids at various operating temperatures.

field during flow. Thus, the ER fluids in this study could not be fully polarized during flow and the structures developed under dc electric field in the absence of flow could not be maintained when the deformation starts, so that initially decreases with $\dot{\gamma}$. In addition, some minor electrophoresis was also reported to be a potential source of this decrease in the case of PANI coated PMMA microsphere systems [41].

For different operating temperatures (20, 40, 60, and 80 °C) of a DBSA-doped polyaniline ER system, the dielectric spectra of Fig. 11(a) and (b) are fitted with the Cole–Cole formula [60] as given in Fig. 12:

$$\varepsilon^* = \varepsilon' + \mathrm{i}\varepsilon'' = \varepsilon'_\infty + \frac{\varepsilon'_0 - \varepsilon'_\infty}{1 + (\mathrm{i}\omega\lambda)^{1-\alpha}} \quad (0 \le \alpha < 1) \tag{8}$$

where ε'_0 is ε' as $\omega \to 0$ ($\varepsilon'_0 = \lim_{\omega \to 0} \varepsilon^*(\omega)$) and ε'_∞ is ε' as $\omega \to \infty$ ($\varepsilon''_0 = \lim_{\omega \to \infty} \varepsilon^*(\omega)$). λ is the relaxation time for the interfacial polarization, and the exponent $(1 - \alpha)$ determines the broadness of the relaxation time distribution. If $\alpha = 0$, this equation represents Debye dielectrics, which have a single relaxation time. It is thought that the difference in the dielectric spectra of our samples is due to varying degrees of polarization. The relaxation

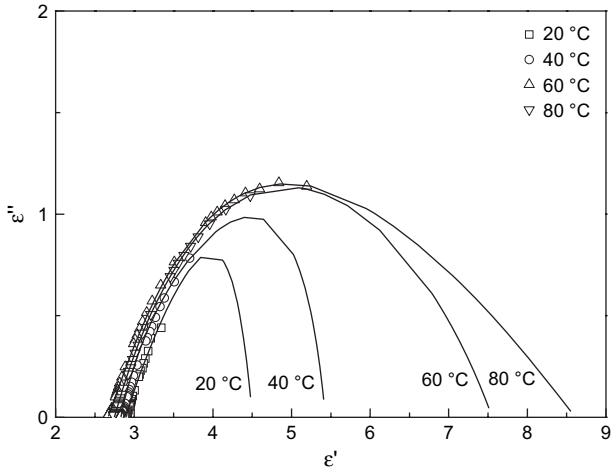

Fig. 12. Cole–Cole plot of 15 wt% DBSA-doped PANI based ER fluids with different operating temperatures (20, 40, 60, and 80 °C).

time of interfacial polarization (λ) and achievable polarizability ($\Delta\varepsilon = \varepsilon_0 - \varepsilon_\infty$) are related with the yield stress and stress enhancement under an applied electric field. τ reflects the rate of interfacial polarization when an external electric field is applied, and thus is mainly related to the stress increase during deformation under a shear field. $\Delta\varepsilon$, meanwhile, shows the degree of polarization of interfacial, dipole-orientation, ionic, and electronic polarization. The polarization rate is inversely proportional to the relaxation frequency. As expected, the magnitude of ε' and ε'' increases with the thermal energy of each particle interaction at different operating temperatures.

The dielectric spectra in Figs. 11 and 12 can also be used to explain the shear stress difference beyond the critical shear rate and yield stress under the electric field, as given in Figs. 5 and 8. The static yield stresses of these ER fluids obtained from Figs. 5 and 8 are proportional to $f_{\max}$, and are consistent with the results of Block et al. [61].

4. Conclusion

DBSA-doped PANI was synthesized as for a suspended particle for ER fluids by emulsion polymerization. The effects of operating temperature on the ER properties of the DBSA-doped PANI suspensions were examined via both rheological and dielectric measurements. The static and dynamic yield stresses were found to increase with both operating temperature and increment of external electric field strength. The yield stress as a function of applied electric field strength showed slopes of 2 and 1.5 from different critical electric field strengths; however, all data points collapse into a universal scaling function. In addition, the dielectric spectra showed the relaxation time with different operating temperatures, confirming the ER performance of DBSA-doped PANI.

Acknowledgement

This work was supported by the KOSEF (R01-2006-000-10062-0) and KRF (D00224-101852, Seo).

References

[1] Tao R, Sun JM. Phys Rev Lett 1991;67:398–401.
[2] Wang BX, Zhao XP. Langmuir 2005;21:6553–9.
[3] Jun JB, Uhm SY, Cho SH, Suh KD. Langmuir 2004;20:2429–34.
[4] Quadrat O, Stejskal J. J Ind Eng Chem 2006;12:352–61.
[5] Kim JW, Kim CA, Choi HJ, Choi SB. Korea–Aust Rheol J 2006;18: 25–30.
[6] Zhao XP, Yin JB. J Ind Eng Chem 2006;12:184–98.
[7] Wu Q, Zhao BY, Fang C, Hu KA. Eur Phys J E 2005;17:63–7.
[8] Wu CW, Conrad H. Phys Rev E 1997;56:5789–97.
[9] Lu KQ, Shen R, Wang XZ, Sun G, Wen WJ, Liu JX. Chin Phys 2006; 15:2476–80.
[10] Huang XX, Wen WJ, Yang SH, Sheng P. Solid State Commun 2006;139: 581–8.
[11] Sung BH, Choi US, Jang HG, Park YS. Colloids Surf A 2006;274: 37–42.
[12] Hiamtup P, Sirivat A, Jamieson AM. J Colloid Interface Sci 2006;295: 270–8.
[13] Pavlinek V, Saha P, Kitano T, Stejskal J, Quadrat O. Physica A 2005;353: 21–8.
[14] Cho MS, Choi HJ, To K. Macromol Rapid Commun 1998;19:271–3.
[15] Ikazaki F, Kawai A, Uchida K, Kawakami T, Edamura K, Sakuri K, et al. J Phys D Appl Phys 1998;31:336–47.
[16] Kuramoto N, Yamazaki M, Nagai K, Koyama K, Tanaka K, Yatsuzuka K, et al. Rheol Acta 1995;34:298–302.
[17] Choi HJ, Kim JW, To K. Synth Met 1999;101:697–8.
[18] Cho MS, Choi HJ, Jhon MS. Polymer 2005;46:11484–8.
[19] Kim JW, Kim SG, Choi HJ, Jhon MS. Macromol Rapid Commun 1999;20:450–2.
[20] Yilmaz H, Unal HI, Sari B. J Appl Polym Sci 2007;103:1058–65.
[21] Maity A, Biswas M. J Ind Eng Chem 2006;12:311–51.
[22] Yoshimoto S. Macromol Rapid Commun 2005;26:857–61.
[23] Cheng Q, He Y, Pavlinek V, Lengalova A, Li C, Saha P. J Mater Sci 2006;41:5047–9.
[24] Cheng Q, Pavlinek V, Li C, Lengalova A, He Y, Saha P. Mater Chem Phys 2006;98:504–8.
[25] Cho MS, Choi HJ, Ahn WS. Langmuir 2004;20:202–7.
[26] Hao T. Adv Mater 2001;13:1847–57.
[27] Kim SG, Kim JW, Choi HJ, Suh MS, Shin MJ, Jhon MS. Colloid Polym Sci 2000;278:894–8.
[28] Österholm J, Cao Y, Klavetter F, Smith P. Polymer 1994;35:2902–6.
[29] Liu Y, Liao FH, Li JR, Zhang SH, Chen SM, Wei CG, et al. Scr Mater 2006;54:125–30.
[30] Wei Y, Sun YJ. J Polym Sci Part A Polym Chem 1989;27:2385–96.
[31] Kang ET, Neoh KG, Tan KL. Prog Polym Sci 1998;23:277–324.
[32] Lee JH, Cho MS, Choi HJ, Jhon MS. Colloid Polym Sci 1999;277: 73–6.
[33] See H, Kawai A, Ikazaki F. Colloid Polym Sci 2002;280:24–9.
[34] Kim YD, De Kee D. AIChE J 2006;52:2350–5.
[35] Shih YH, Conrad H. Int J Mod Phys B 1994;8:2835–53.
[36] Cho MS, Choi HJ, Chin IJ, Ahn WS. Microporous Mesoporous Mater 1999;32:233–9.
[37] Yin J, Zhao X. Chem Mater 2006;18:2773.
[38] Dong P, Wang C, Zhao S. Fuel 2005;84:685–9.
[39] Sprecher AF, Carlson JD, Conrad H. Mater Sci Eng 1987;95:187–97.
[40] Parthasarathy M, Klingenberg DJ. Mater Sci Eng 1996;R17:57–103.
[41] Cho MS, Cho YH, Choi HJ, Jhon MS. Langmuir 2003;19:5875–81.
[42] Park SJ, Cho MS, Lim ST, Choi HJ, Jhon MS. Macromol Rapid Commun 2005;26:1563–6.
[43] Kim YD, Park DH. Synth Met 2004;142:147–51.
[44] See H. J Phys D Appl Phys 2000;33:1625–33.
[45] Brunn PO, Abu-Jdayil B. Rheol Acta 2004;43:62–7.
[46] Wu C, Chen Y, Conrad H. J Phys D Appl Phys 1998;31:960–3.
[47] Hao T, Kawai A, Ikazaki F. Langmuir 1998;14:1256–62.
[48] Davis LC. J Appl Phys 1997;81:1985–91.
[49] Choi HJ, Cho MS, Kim JW, Kim CA, Jhon MS. Appl Phys Lett 2001;78: 3806–8.
[50] Sim IS, Kim JW, Choi HJ, Kim CA, Jhon MS. Chem Mater 2001;13: 1243–7.
[51] Ma Y, Zhang YL, Lu KQ. J Appl Phys 1998;83:5522–4.
[52] Gonon P, Foulc JN. J Appl Phys 2000;87:3563–6.
[53] Hao T, Yu H, Xu YZ. J Colloid Interface Sci 1996;184:542–9.
[54] Wu CW, Conrad H. J Phys D Appl Phys 1998;31:3403–9.
[55] Wei JH, Shi J, Liu ZY, Guan JG, Yuan RZ. Int J Mod Phys B 2005;19: 1423–9.
[56] Jordan TC, Shaw MT, Mcleish TCB. J Rheol 1992;36:441–63.
[57] Ferry JD. Viscoelastic properties of polymers. New York: Wiley; 1980.
[58] Negita K, Ohsawa Y. J Phys II (Paris) 1995;5:883–92.
[59] Uejima H. Jpn J Appl Phys 1972;11:319–26.
[60] Fannin PC, Giannitsis AT. J Mol Liq 2004;114:89–96.
[61] Block H, Kelly JP, Win A, Watson T. Langmuir 1990;6:6–14.